Substructure Testing and Structural Optimisation of a Wind Turbine Blade Web Bond Detail

B. Saurdal, J. Bjoner, M. Steffensen, N. Gripon, P. Broberg, R. Hole

Department of Materials and Production, Aalborg University
Fibigerstraede 16, DK-9220 Aalborg East, Denmark
Email: [bsaurd18, jbjone18, msteff15, ngripo19, pbrobe15, rhole18]@student.aau.dk,
Web page: http://www.mechman.mp.aau.dk/

Abstract

This paper aims to increase knowledge and provide sufficient documentation to certify a web bond joint inside a wind turbine blade. A problem analysis is done from an original design provided by an industrial partner. This gives knowledge for concept design generation to find an initial design for the project. The initial design is tested and optimised to achieve an improved design. New tests and calculations are done, and a static failure criteria is established.

Keywords: Wind turbine blade, shear web, web bond, optimisation, experimental mechanics

Nomenclature

FE	Finite Element
VARTM	Vacuum Assisted Resin Transfer Moulding
UD	Unidirectional
FI	Failure Index
BC	Boundary Condition
DEL	Damage Equivalent Load
CLT	Classic Lamination Theory

1. General Introduction

The trend seen in wind energy today is that the blades are getting bigger to maximise their efficiency [1]. With this trend there are some challenges. One of which is the lack of knowledge on the strength of the web bond joint between the shear web and outer shell of the blade (Fig. 1). This lack of knowledge is indirectly reflected in the most recent design guideline for wind turbine blades, where it is strongly recommend to carry out substructure tests on critical components [2] [3].

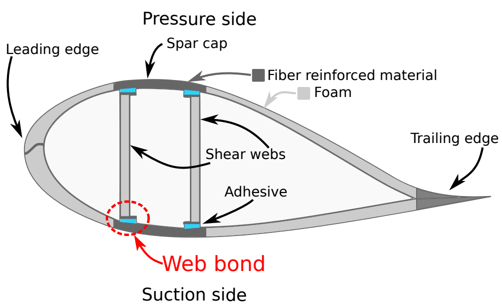

Fig. 1 Simple cross section of the general structure of a wind turbine blade with two shear webs.

As different blade manufacturers use different solutions [4] [5], it is desired to come up with a well documented design for the detail.

An important aspect in the blade design is the certification. In the current standard, *Rotor blades for wind turbines* (DNVGL-ST-0376), there are no requirements directly defining the design of the web bond joint [2]. This paper has been made together with an industrial partner, who desires this detail studied and potentially improved for new blade designs. Thus the aim of this paper is to provide design guidelines and optimised parameters of the web bond detail of a wind turbine blade.

2. Methods

In this section the methods used for improving the design of the web bond will be described. Methods are described to make the results reproducable. A detailed description of the methods can be found in the appendix report.

2.1 Full Blade Modelling

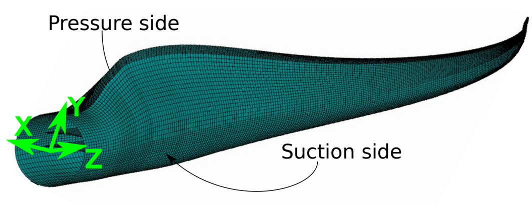

Fig. 2 Illustration of the blade model along its pressure side (PS). Hidden is the suction side (SS).

The industrial partner provided a FE model of a generic blade (Fig. 2), as well as a load envelope of four load cases: Max/min flapwise and edgewise bending.

2.1.1 Study of the Influence of Parameters

A study on how the parameters for the web bond influence the load transferred through the web bond was carried out. This was done as it is of interest to know how parameters in the web bond changes these loads. The varied parameters were core thickness, face sheet thickness and web foot thickness (Fig. 3 a).) The loads transferred from the outer shells to the shear web through the web bond are peel force (N_{11}), shear force (Q_{13}) and bending moment (M_{11}) (Fig. 3 b).).

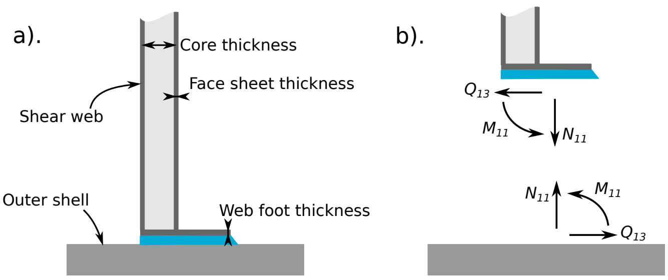

Fig. 3 a). Illustration of parameters changed in the analysis of the loads through the web bond. b). Forces transferred from the outer shell to the shear web through the web bond.

An analysis on how these parameters impact the transferred loads was performed by a variation of the values in ANSYS. The analysis considered factors of 0, 0.5, 1, 2 and 4 times the original thickness of the parameters. Only the elements along the edges of the shear web were subjected to this change, thus simulating changes in the web foot.

2.2 Concept Design Generation

Systematic design generation was used to come up with a concept design for the improved web bond. The morphological approach was used to come up with possible solutions, described by M. M. Andreasen [6].

2.2.1 Manufacturing Constraint and Design Objectives

The solutions, derived by the morphological approach, were imposed by the manufacturing constraint, that it should be manufacturable by use of the shear web mould described in Sec. 2.3.1. All solutions obtained by the morphological analysis were screened by the manufacturing constraint to remove solutions that were not manufacturable.
The rest of the solutions were rated based on the design objectives. The design objectives, method of rating and weighing of design objectives were:

- **Mass**. Evaluated qualitatively by how much material was needed for the solution. Weighed 2.
- **Cost**. Evaluated qualitatively by what material and processing the solution needed. Weighed 3.
- **Manufacturability**. Evaluated qualitatively by how easy the solution would be manufactured in the shear web mould. Weighed 5.
- **Failure modes**. Evaluated qualitatively by what failure modes the solutions was prone to experience. Weighed 4.
- **Tolerances**. Evaluated qualitatively by what tolerances the solution needed to function. Weighed 1.

The solution that got rated the highest was chosen as the initial design (Fig. 4). The design obtained from the optimisation on the initial design (Sec. 2.5) will later be termed the redesign.

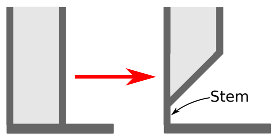

Fig. 4 Change from original to initial design.

2.3 Experimental testing

To verify models used in the paper and come up with a failure criteria, experimental tests were performed on self-manufactured specimens of the initial design and later the redesign. In order to compare the loads, they're changed to N/mm in Sec. 4.

2.3.1 Specimen Manufacturing

The test specimens consist of two parts, the spar cap and the shear web. Both are produced by VARTM, a composite production technique (Fig. 5). This method is thoroughly described in the appendix report. For the production of the test specimens Airstone resin (760E/766H) was used.

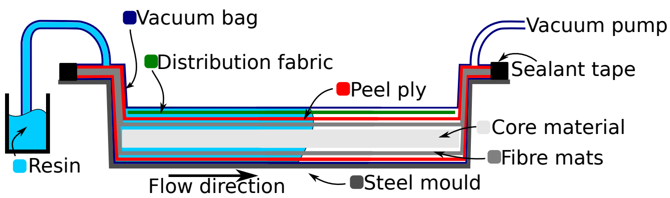

Fig. 5 Vacuum assisted resin transfer moulding layup.

The spar cap part was not intended to represent the full size spar cap, it was only supposed to have

sufficient stiffness to be assumed rigid. The layup was: $[(\pm45°/90°)_5\ /\ 0°_{10}]_s$, where the $(\pm45°/90°)$ layers were TRIAX 1200 glass fibre mats, and the 0° layers were UD 1200.
The shear web main layup was $[(\pm45°)_4/\mathrm{H100}/(\pm45°)_4]$, where the $\pm45°$ layers were BIAX 600 glass fibre mats, and H100 was a 30 mm thick PET foam core. A metal mould with a 90° flange was used to create the foot of the web.
After the two specimen plates were produced, they were cut into 40 mm thick and 420 mm high specimens and glued together using an adhesive (Epikote MGS BPR 135G3/Epicure MGS BPH 137G)

2.3.2 Test Modes and Setup

The specimens were tested in four modes: tension, compression, and positive/negative bending. For all tests the spar cap was clamped to a steel plate (Fig. 6).

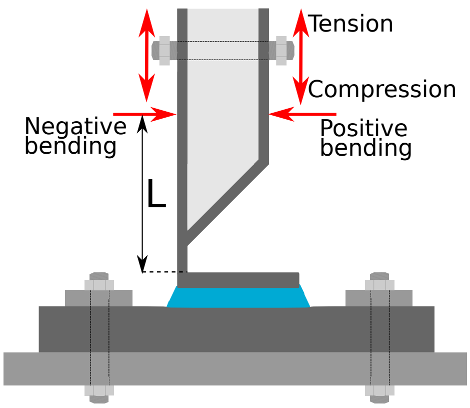

Fig. 6 Test setup for tension/compression by applying force vertically on the bolt. The horizontal arrows indicate load application at a distance L for positive and negative bending.

Positive bending is defined as bending away from the web foot, (Fig. 6).
The test machine used was given to have uncertainties for the load cell and displacement transducer of 0.1 % and 1 %, respectively.

2.3.3 Strain Gauges

To check the validity of the submodel described in Section 2.4, two strain gauges were used. They were intended to measure the strain in the y-direction, and were positioned in the centre of the web, 20 mm above the end of the core tapering.
From knowledge about strain gauge theory and the Wheatstone bridge, it can be shown that the indicated strain ε_i' is related to the strain gauge factor K_{SG} and change in output voltage V_o relative to the excitation voltage V_S by the equation:

$$d\left(\frac{V_o}{V_S}\right) = \frac{K_{SG}}{4}\cdot\varepsilon_i' \tag{1}$$

Inserting Eq. (1) into the power product rule [7] as shown in the appendix report, the following expression for strain gauge uncertainty is obtained:

$$\frac{s\left(\varepsilon_i\right)}{\varepsilon_i} = \sqrt{\left(-1\cdot\frac{s\left(K_{SG}\right)}{K_{SG}}\right)^2 + \left(\frac{s\left(d\left(\frac{V_0}{V_S}\right)\right)}{d\left(\frac{V_0}{V_S}\right)}\right)^2} \tag{2}$$

Mouritsen [7] states that the second term under the square root in Eq. (2) will be negligible compared to the uncertainty of the strain gauge factor.

2.4 Submodelling

A submodel of the web bond was made in ANSYS in order to optimise the intial design and get a more accurate assesment of the failure modes. The model was made using ANSYS's solid shell elements SOLSH190. The mesh size was found from a global deflection convergence study to be 3 mm. The geometry and material used for the submodel are described in the appendix report.
In order to match the experimental load case, the submodel was fixed at the bottom of the spar cap and the top of the shear web was constrained against rotation and translation along the x-direction (Fig. 7).

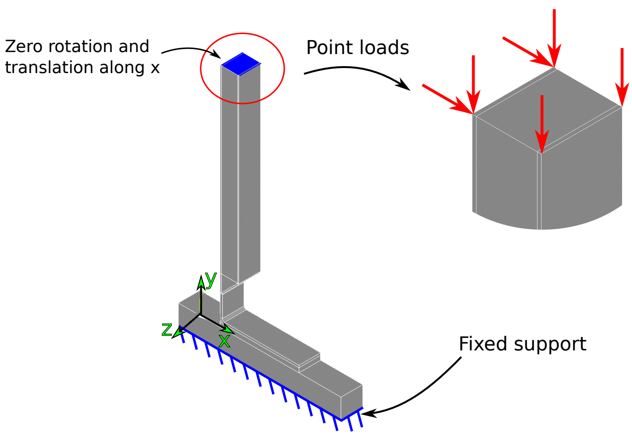

Fig. 7 Illustration of the BC's and loads applied to the submodel. Red symbols indicates loads applied and blue symbols indicates BC's.

The loads were applied at the top of the shear web as point loads (Fig. 7).
For the optimisation, the submodel was altered to include three changeable parameters: the stem height h_s, stem thickness t_s and foot length L_f (Fig. 8)

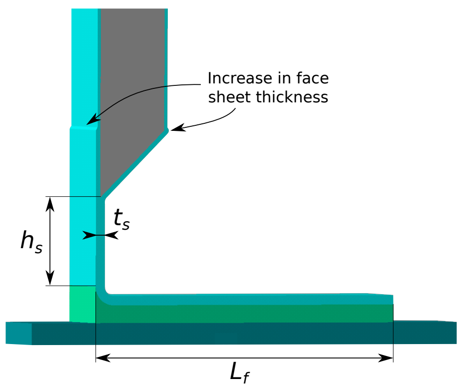

Fig. 8 Illustration of the altered submodel, that includes the three design variables: stem height h_s, stem thickness t_s and foot length L_f.

2.5 Optimisation

To improve the mechanical properties of the initial design, the new design was optimised. The parameters used for the optimisation were the three design variables described in Sec. 2.4:

$$x_1 = h_s, \qquad x_2 = t_s, \qquad x_3 = L_f \tag{3}$$

The design was optimised with respect to the max stress failure criteria obtained from the ANSYS submodel loaded with 10 kN in compression. The objective function was the p-norm of the 500 largest FI's in the model, see Eq. (4).

$$f_{PN}(\mathbf{x}) = \left(\sum_{k=1}^{n_0} (f_k)^p \right)^{1/p} \tag{4}$$

In Eq. (4) n_0 is the number of FI's used, f is a vector containing the 500 FI's, and p is set to 10.
Four requirements were set up for the constraint functions:

- *Requirement 1:* The mass of the new design must not exceed the mass of the original design.
- *Requirement 2:* Extra BIAX layers added to the stem must not exceed twice the number of layers in the face sheets.
- *Requirement 3:* The height of the stem must be larger than 5 mm.
- *Requirement 4:* The length of the foot must be larger than 50 mm.

Translated to mathematical statements, the four constraint functions were:

$$\begin{aligned} g_1(\mathbf{x}) &= x_2 - 4t_{fs} < 0 \\ g_2(\mathbf{x}) &= 0.005 - x_1 < 0 \\ g_3(\mathbf{x}) &= 0.05 - x_3 < 0 \\ g_4(\mathbf{x}) &= m_0 - m(\mathbf{x}) < 0 \end{aligned} \tag{5}$$

Where m_0 is the original mass of the web foot while $m(\mathbf{x})$ is the mass of the web foot with the given design variables $\mathbf{x}$.
The final optimisation problem was formulated as:

$$\begin{aligned} &\min f(\mathbf{x}) \\ \text{Subject to} \quad &g_i(\mathbf{x}) \leq 0, \quad i = 1, 2, 3, 4 \end{aligned} \tag{6}$$

As this is a nonlinear problem the sequential quadratic programming (SQP) algorithm was used [8].
The design obtained from the optimisation is referred to as the redesigned web bond.

2.6 Verification Analyses

Verification analyses were performed to validate if the redesigned concept is viable for use in future wind turbine blades. The methods used for validation is fatigue life estimation, linear buckling analysis and estimation of static failure envelope.

2.6.1 Fatigue Life

Fatigue life was estimated by first obtaining SN-curves for the adhesive and composite face sheets.
Adhesive: The adhesive SN-curve was obtained by applying the Basquin equation (Eq. 7) to the material properties of the adhesive, provided by the blade manufacturer.

$$S = A \cdot N^{-\frac{1}{m}} \tag{7}$$

In the equation S is fatigue strength, A is a proportional scaling factor, N is number of cycles and m is the slope of the SN-curve.
Face sheets: For the face sheets, two separate SN-curves were obtained, one for stress in material direction one and two (S11 / S22), and one for in plane shear stress (S12). The face sheets are $\pm 45°$ laminates and therefore assumed to have negligible difference in fatigue strength in directions 1 and 2. The SN-curve for S11 / S22 was based on data lifted from the Upwind fatigue database [9].
As fatigue data for relevant laminates was not available, a different approach was used to obtain the SN-curve for S12. Loading a $\pm 45°$ laminate in shear can be approximated as loading it along the two fibre directions for a [0,90] laminate, as shown in the appendix report.

Data from the same database was curve fitted to obtain the slope of the SN-curve. The exact data lifted for both curves can be found in the appendix report. The proportional scaling factor was set as the ultimate shear strength of the shear web laminate. Due to the approximation, both the 95% confident bonds of the slope and the scaling factor is used to make the curve more conservative.

After obtaining the SN-curves the resulting stress amplitudes from the provided DEL's were obtained from the full blade model. The stress amplitudes for the original design were obtained by first applying the DEL's to the full blade model and finding the element with the highest peel force. Then exporting the CLT-forces of the element into a submodel. The highest stress values for S11, S22 and S12 were then inserted into the appropriate SN-diagrams. For the new design, the same approach was applied to the modified full blade model.

2.6.2 Buckling Analysis

A linear buckling analysis was carried out on the ANSYS submodel. As the buckling load factor is dependent on the height of the submodel, the analyses was carried out on heights corresponding to different lengths along the blade (Tab. I).

L [m]	4.5	8.0	12.0	17.0	21.3	28.5	37.5
h_{SW} [m]	2.3	1.9	1.6	1.2	1.0	0.7	0.4

Tab. I Heights of the shear web used for the buckling analysis. L is the length along the full blade and h_{SW} is the corresponding height of the shear web.

To limit the size of the model used for the buckling analysis, only half the height of the shear web was used and symmetry was used by constraining the top of the model against rotation.

A fit was made to the obtained values of buckling load, to get a buckling criteria along the blade.

2.7 Failure Envelope

A failure envelope based on the experimental results was made for the web bond. This is based on the tensile peel strength $S_{Peel,t}$, compressive peel strength $S_{Peel,c}$, positive bending strength S_{Bend+} and negative bending strength S_{Bend-}. The failure envelope was based on a linear relationship between the strengths as this yields conservative failure predictions compared to a max load failure envelope (Fig. 9).

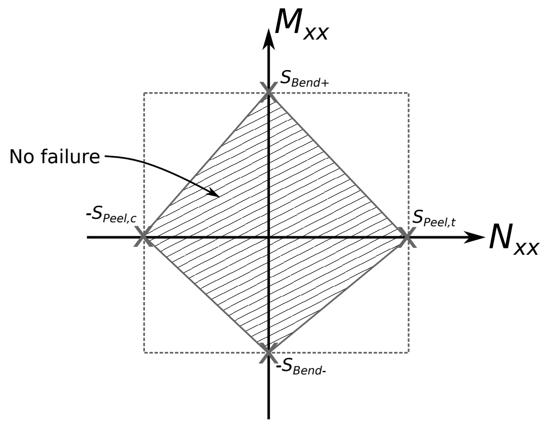

Fig. 9 Illustration of the failure envelope used. The stippled box is a max load envelope and the shaded box is a linear failure envelope.

The failure envelope was used on a modified model of the blade model, that includes the new web bond design. The alterations made to the blade model is described in the appendix report.

3. Results

This section contains the results found through tests and analyses using the methods from Section 2. Only results relevant for the discussion will be presented here. Other results are included in the appendix report.

3.1 Full Blade Model

The following graphs show the load cases for one shear web joint line. The results in this subsection are for the original web foot design. The peel force transferred through the web bond was largest in the beginning of the shear web, with a value of approximately $1 \cdot 10^5$ N/m and then decreased along the blade. The compressive peel forces did not get below $-5 \cdot 10^4$ N/m. Due to singularities in the full blade model peaks were present in the peel forces (Fig. 10).

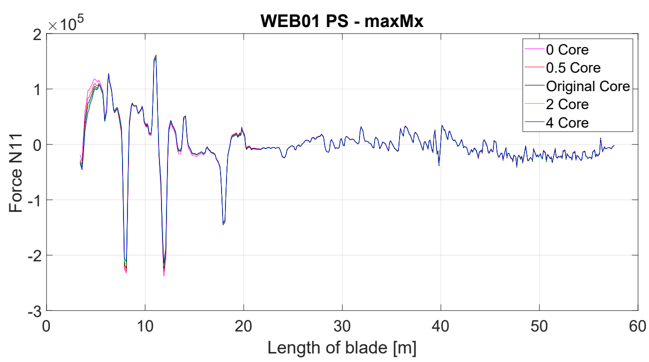

Fig. 10 Peel force through the length of the blade for different core thicknesses.

The bending moment transferred by the web bond had a maximum value of 3000 N around 8 m along the blade. It then decreased to a value of -800 N, 40 m along the blade and approached 0 at the end of the blade (Fig. 11).

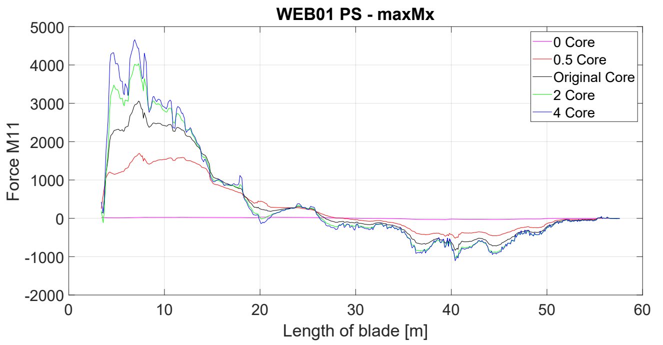

Fig. 11 Bending moment through the length of the blade for different core thicknesses.

By changing the core thickness of the web bond elements the peel force remained unaffected (Fig. 10). This was the trend when changing the other parameters, as can be seen in the appendix report. The bending moment approached 0 along the whole blade for 0 core thickness, and increased to a maximum value of around 4500 N with four times the original core thickness (Fig. 11).

By changing the face sheet thickness of the web bond elements the maximum bending moment increased to 4000 N and the minimum bending moment decreased to -1000 N for four times the original face sheet thickness (Fig. 12).

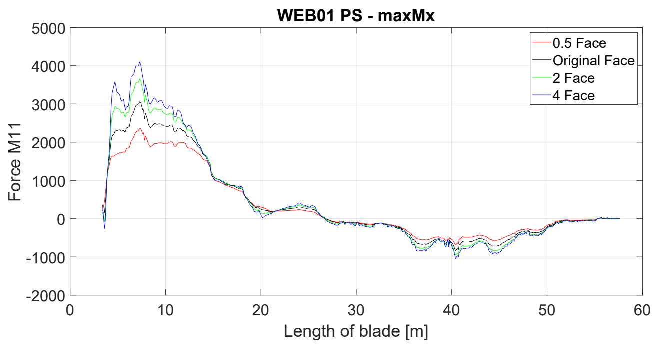

Fig. 12 Bending moment through the length of the blade for different face sheet thicknesses.

Increasing or decreasing the web foot thickness did not affect the minimum or maximum value of the bending moment but slightly changed the bending moment in the middle of the blade.

3.2 Validation of Submodel

In this subsection the results from the comparison of the submodel and strain gauges on the initial design will be presented.

The strain gauges on the specimen in tension measured a linear relationship between displacement and strain with a slope of 0.00190 Strain/mm and 0.00044 Strain/mm for the rear and front face strain gauge respectively. The submodel predicted a slope of 0.00200 Strain/mm at the location of the rear strain gauge and 0.00024 Strain/mm at the location of the front strain gauge. Thus the submodel deviates with 6.42 % at the rear strain gauge and -44.9 % at the front strain gauge (Fig. 13).

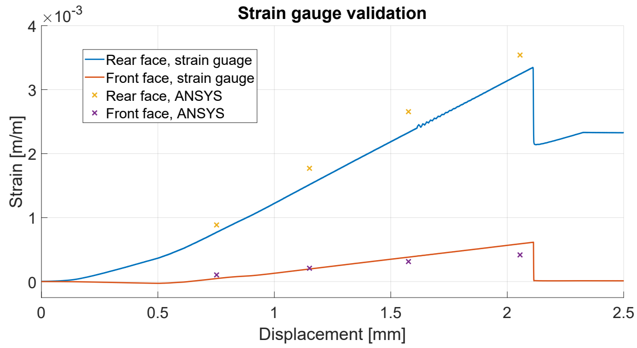

Fig. 13 Strain comparison of strain gauge values and values from FEA in ANSYS.

The strain gauge factor is given as $K_{SG} = 2.155 \pm 0.5\%$. This yields an uncertainty for the indicated strain gauge strain on 0.232 % by use of Eq. 2.

3.3 Optimisation

The optimiser converged after three iterations and yielded the parameter values shown in Tab. II. These parameters is what is used for the redesign.

x_1	x_2	x_3
0.005 [m]	0.008 [m]	0.05 [m]

Tab. II Results from the optimisation.

3.4 Experimental Testing

Two tests were done per test mode for both the initial design and the redesign. The strength for the specimens with the lowest strength for a given test mode is compared. Strength is defined as the maximum load before the force applied drops the first time.

In tension the redesign failed at 12 kN (8.5 mm), while the initial design failed at 6 kN (3.5 mm) (Fig. 14).

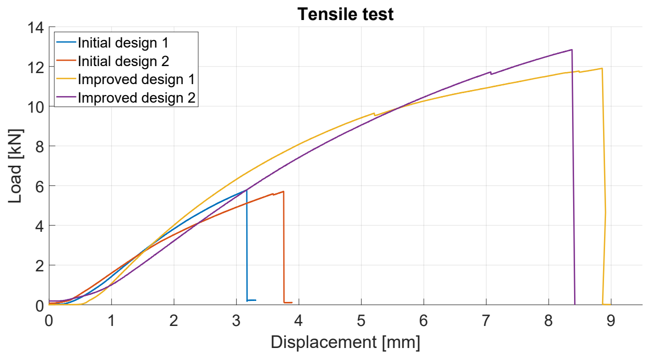

Fig. 14 Initial design and redesign tested in tension.

In compression the redesign failed at 8.1 kN (5 mm), while the initial design failed at 4 kN (3.5 mm). (Fig. 15)

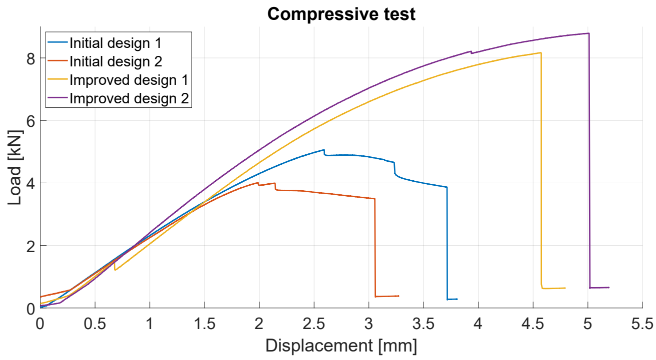

Fig. 15 Initial design and redesign tested in compression.

The redesigned specimens tested in tension failed in the adhesive layer with a complete separation of the shear web and spar cap. In compression the redesign failed by a crack in the tapering of the core material, which propagated to the face sheets (Fig. 16).

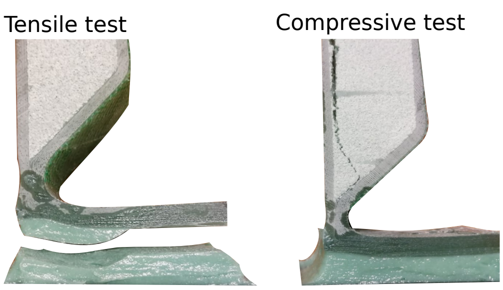

Fig. 16 Tension and compression failure modes.

In positive bending the redesign failed at 51 Nm (46 mm) and the initial design reached the machine limit (160 mm) at 11.3 Nm without failing (Fig. 17).

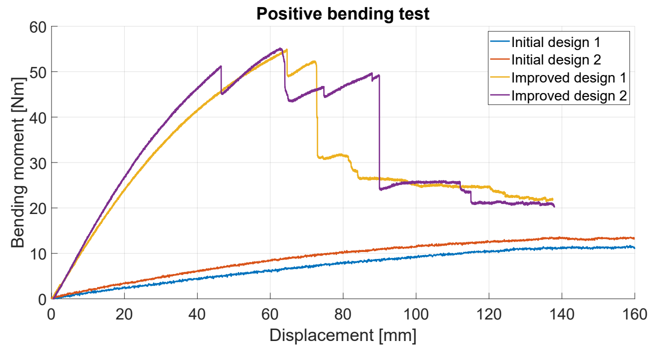

Fig. 17 Initial design and redesign tested in positive bending.

In negative bending the redesign experienced some local failure for 36 Nm at 27 mm displacement but increased to 60 Nm after 160 mm displacement. The initial design reached the machine limit (160 mm) at 10 Nm without failure.

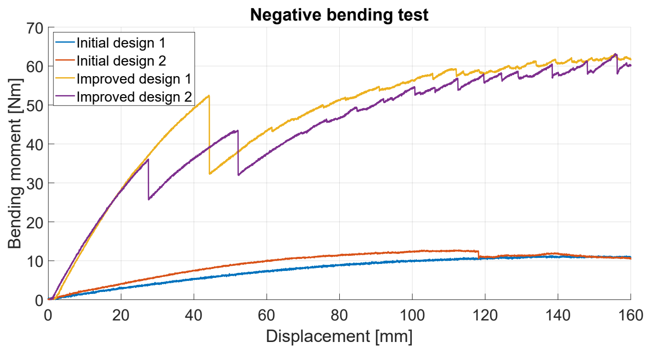

Fig. 18 Initial design and redesign tested in negative bending.

In positive bending the specimens failed by delamination at the stem of the web foot, which started a crack propagating through the core. In negative bending the specimens failed with a crack starting in the tapering of the core material, then propagating to the face sheets (Fig. 19).

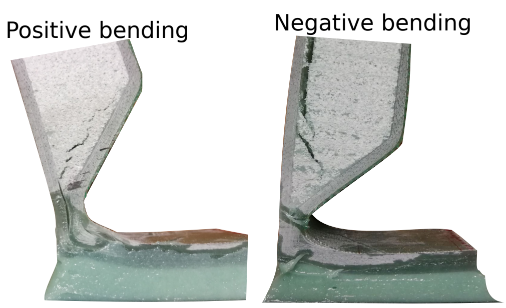

Fig. 19 Failure modes for positive and negative bending.

3.5 Loads from Modified Blade Model

The maximum peel forces obtained from the modified blade model was, when ignoring peaks, around $1 \cdot 10^5$

N/m at 5 m along the blade. Further down the blade they decreased (Fig. 20).

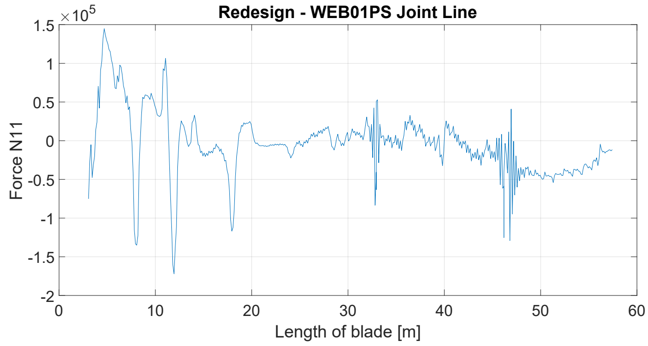

Fig. 20 Peel force transferred in the modified blade model.

The bending moment obtained from the modified blade model had a lot of peaks. The maximum bending moment was around 1500 N while the minimum was -500 N (Fig. 21)

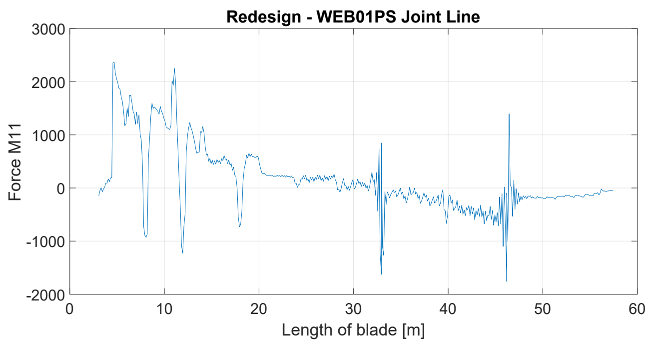

Fig. 21 Bending moment transferred in the modified blade model.

3.6 Verification

3.6.1 Buckling

The buckling load is lowest at the start of the shear web. In this location, the buckling load of the new design is approximately 56 % of the original design. As the shear web height increases, this ratio increases to 92 % at the other side of the shear web (Fig. 22).

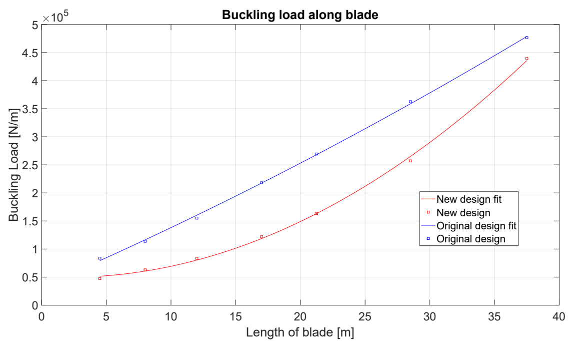

Fig. 22 Results from the buckling analysis.

By disregarding the peaks in the peel forces, the buckling load factor was above 1 along the whole shear web when comparing the new peel forces with the buckling load (Fig. 20 and Fig. 22).

3.6.2 Fatigue Life

The SN-curve with respect to S11 and S22 along with the maximum stress amplitudes, for both the original and the redesign is shown in Fig. 23. Estimated fatigue life for the face sheets and the adhesive is listed in Tab. III.

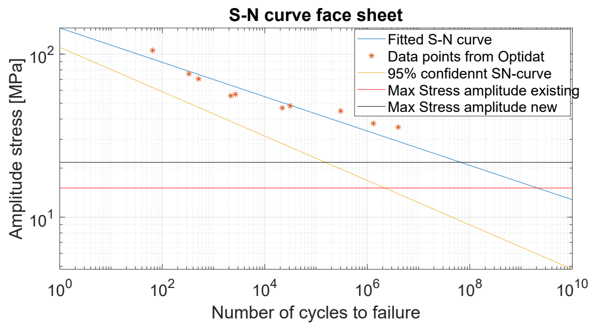

Fig. 23 SN-curve for S11 and S22 in face sheets.

Stress amplitude	Cycles (failure)	Cycles (failure 95%)
S11 / S22 original	2.094E9	2.197E6
S12 original	5.262E23	2.083E20
S11 / S22 new	6.616E7	1.517E5
S12 new	5.500E21	3.900E18
Adhesive original	—	3.387E5
Adhesive new	—	5.760E8

Tab. III Estimated fatigue life of the face sheets and the adhesive, for both the original and new design.

3.7 Failure Envelope

The failure load envelope with the loads from the full blade model is shown in Fig. 24.

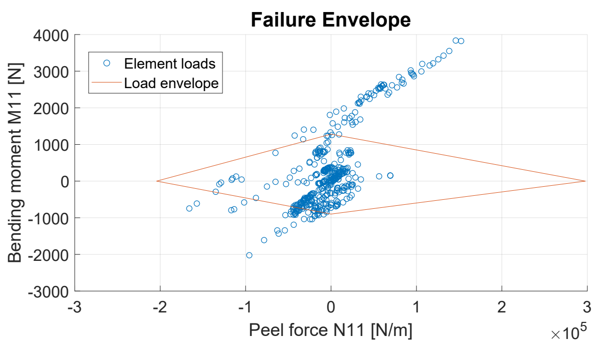

Fig. 24 Conservative failure envelope with element loads.

Most of the points from the full blade model are inside the failure criteria. However, for several points, especially due to the bending moment, failure is predicted.

4. Discussion

From the loads transferred through the web bond, it is clear that a lower bending stiffness of the web bond is preferable as it lowers the bending moment while keeping the peel forces the same. This is due to the outer shells carrying the applied load, while the moment transferred through the web bond is governed by the deformation of the outer shells. Hence a lower stiffness of the web bond transfers less moment.

The observation of the bending moment is one of the key reasons to why the soft hinge concept was chosen in the morphological analysis. By transferring less moment to the shear web, the failure indices for the shear web will consequently be lower.

From the results of the experimental bending tests of the initial design, it was observed that the deflection of the shear web reached the limit of the testing machine without failure. This excessive deformation will however not happen in the real shear web unless it buckles. Therefore, it is safe to assume that the initial design will not fail in bending. For the compressive test, the initial design failed with a loading of 4 kN which is equivalent to a load per unit of 100 N/mm. Disregarding the peaks in Fig. 10, the maximum compressive loading does not exceed 50 N/mm, which implies that the initial design will not fail due to compressive loading either. The shear web might however fail in buckling due to compressive loading. This will be discussed later. In the tensile test, the initial design failed in the adhesive at 5.7 kN equivalent to 142.5 N/mm. This is only slightly higher than the maximum peel force the web bond experience in Fig. 10. Keeping in mind that the load comparison between the model and the experimental results does not take load interactions into account, the optimisation was carried out to increase the safety factor. To sum up, the initial design removes failure modes related to bending, but might result in adhesive failure due to peel forces.

The submodel is deemed valid after the comparison of the submodel and experimental strain gauge measurements in Fig. 13, because the models response only deviated with 6.42 % for one strain gauge. For the other it deviated with -44.9 %. This large deviation could however be due to the relatively low signal obtained from strain gauge.

The objective function of the optimisation was FI for the submodel in compression. This was chosen since the initial design experienced failure in the adhesive under tensile loading. As the thickness and shape of the adhesive layer is unchangeable due to manufacturing constraints, the adhesive failure was first thought of as being non changeable. After the optimisation the thickness of the stem is doubled and the foot length and stem height were reduced. Intuitively it makes sense to move material from the web foot to the stem in order to lower the failure criteria that originated from the stem (Fig. 16) and the optimisation is therefore accepted.

From the results of the redesigned web bond it is observed that the compressive strength is increased from 4.0 kN to 8.1 kN equivalent to 202.5 N/mm. As the design is optimised with respect to compressive failure, these results makes sense. It was furthermore observed that the tensile strength increases from 5.7 kN for the initial design to 11.9 kN equivalent to 297.5 N/mm. This means that the strength of the adhesive bond is not just dependent on the shape of the adhesive layer, but also the number of layers in the web foot. An explanation to this is that the stiffer web foot distributes the stresses from the peel forces more evenly over the adhesive layer, than the more compliant initial design. From these test a linear relationship between number of layers and peel strength may be assumed, however more test are needed to validate this. Furthermore, it is also observed that the slope of the response of both the initial and redesigned web bond in compression and tension are approximately the same (Fig. 14 and Fig. 15). This implies that the axial stiffness of the web bond hasn't changed remarkable with the added layers of BIAX in the stem. This observation further validates the results from the full blade analysis, where it was shown that face sheet thickness in the web foot did not change the peel force transferred. The bending of the redesigned web bond showed a much stiffer response than the initial (Fig. 17 and Fig. 18), which is due to the added layers of BIAX. This results in the specimens failing at 27.5 mm of displacement for negative bending and 46.1 mm for positive bending with a moment equivalent to 902.5 N and 1270 N, respectively. It is thus no longer safe to assume that the web bond does not fail in bending.

From the established failure envelope it was shown that the web bond will not fail due to peel forces in the modified blade model. However, the bending moment obtained from the modified blade model contains many peaks due to the singularities in the model. This explains why failure is predicted in some points on the shear web. Furthermore, the transferred bending moment for the modified blade model is the same size as for the original model. As it is expected that the soft hinge design lowers the bending moment transferred, this indicates that the model predicts the wrong moment transferred. Investigation of the modified full blade model or experimental comparison of bending stiffness of the new and original design is needed to conclude if the new design fails due to short term loading.

The results from the fatigue analysis showed a significant decrease in fatigue life for the face sheets of the redesign compared to the original one. The decrease was most likely caused by a stress concentration in the face sheets, due to the ply drops. Additionally the adhesive of the redesign showed improved fatigue life. This was believed to be because the redesigned web bond transfers less bending moment, thus reducing the peeling effect on the adhesive. Also, the stiffened web foot could be distributing the stress more uniformly through the adhesive.

The results from the buckling analysis showed that the buckling load factor approached 1 at the beginning of the shear web. For a normal linear buckling analysis this would be critical. Since the analysis was carried out on the submodel, which does not take into account the continuity of the shear web, the buckling analysis is conservative. The redesign has a buckling load factor about half of the original design. This means that the soft hinge design has severely decreased the buckling resistance. Due to the conservative buckling analysis and the redesign lowering the buckling load factor, further buckling analyses are needed in order to ensure that the redesign does not fail in buckling.

5. Conclusion

In this paper a new design to the web bond of a wind turbine blade has been investigated. This proposed design utilises a soft hinge, which results in a reduction of bending moment being transferred from the outer shells of the blade to the shear web. The new design predicts no failure in tension and compression for the given generic blade model. However, modifications made to the blade model yielded inconclusively results on the transferred bending moment. Further investigation is thus needed to predict if the new design fails due to bending in the blade model. A complete static failure envelope for this design has been described in this paper, and may be used on future design of wind turbine blades or future research on the web bond detail. However, for the design to be used in a wind turbine blade, further testing or analyses are needed on buckling failure.

Acknowledgement

The authors of this work gratefully acknowledge Grundfos for sponsoring the 7$^{\text{th}}$ MechMan symposium.

References

[1] DNVGL, "Third generation wind power." Online Article - https://www.dnvgl.com, 2019.
[2] DNVGL, DNVGL-ST-0376 Standard, 2015.
[3] GL, Guideline for the Certifiation of Wind Turbines, 2010.
[4] C. Flach. Patent no. US20110229333A1 - https://patents.google.com/, 2011.
[5] A. Yarbrough. Patent no. US8235671B2 - https://patents.google.com/, 2012.
[6] M. M. Andreasen, "Systematiske idemetoder," Konstruktionsteknik/DTH, vol. Problemløsning, pp. 11–21, 1984.
[7] O. Ø. Mouritsen, "Basic uncertainty evaluation by measurements using strain gages," 2013.
[8] J. Nocedal and S. J. Wright, Numerical Optimization. Springer, 1999.
[9] Nijssen, R.P.L, OptiDAT - fatigue of wind turbine materials database. http://www.www.kc-wmc.nl, 2011. Downloaded: 09-05-2019.